Mechanical and Environmental Stability of Polymer Thin-Film-Coated Graphene

Chao Yan,[†,#] Kwang-Seop Kim,[‡,#] Seoung-Ki Lee,[†] Sang-Hoon Bae,[†] Byung Hee Hong,[§] Jae-Hyun Kim,[‡] Hak-Joo Lee,[‡] and Jong-Hyun Ahn[†,*]

[†]SKKU Advanced Institute of Nanotechnology (SAINT) and Center for Human Interface Nano Technology (HINT), School of Advanced Materials Science and Engineering, Sungkyunkwan University, Suwon 440-746, Korea, [‡]Department of Nano Mechanics, Nano Convergence and Manufacturing Systems Research Division, Korea Institute of Machinery & Materials, 104 Sinseongno, Yuseong, Daejeon, 305-343, Korea, and [§]Department of Chemistry, Seoul National University, Seoul 151-747, Korea. [#]C. Yan and K.-S. Kim contributed equally to this work.

ABSTRACT

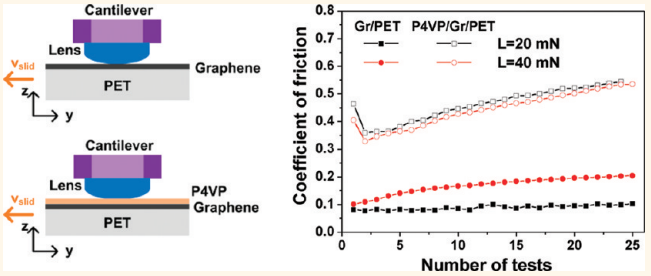

A uniform polymer thin layer of controllable thickness was bar-coated onto a chemical vapor deposition (CVD) grown monolayer graphene surface. The effects of this coating layer on the optical, electric, and tribological properties were then investigated. The thin polymer coating layer did not reduce the optical transmittance of the graphene films. The variation in the sheet resistance of the graphene films after the coating depended on the interaction between polymer and graphene. The top coating layer can maintain the high conductivity of chemical doped graphene films under long-term ambient conditions compared with uncovered doped samples. Friction tests demonstrated that the polymer coating layer can enhance both the friction force and the coefficient of friction of the graphene films and protect the graphene against damage in the repeated sliding processes.

KEYWORDS: CVD-grown graphene · encapsulation · bar coating · polymer thin film · sheet resistance · friction

As the market for optoelectronic devices such as flat panel displays, solar cells, and touch screen panels continuous to grow, the demand on transparent conductive materials is also increasing. Indium tin oxide (ITO) has been dominantly used for transparent conductive materials due to its good transparency and excellent conductivity. However, problems such as the limited supply of indium, the instability, and the poor mechanical properties of these metal oxides have resulted in the search for alternatives with good transparency, conductivity, and stability. Metal wires,[1−3] carbon nanotubes,[4−7] conductive polymers[8,9] and graphene[10−15] have been exploited as alternatives to ITO films.[16] Among them, ultrathin graphene films have attracted interest due to their good conductivity (50−400 Ω/sq at optical transmittance over 90%), extraordinary mechanical properties (Young's modulus ≈ 1 TPa), chemical stability, and patternability.[17−21] Recent works for producing large-area, high quality graphene films through chemical vapor deposition (CVD) and transferring them onto various large-area substrates have offered the possibility of their use as transparent conductive films in optoelectronic devices.[22−24] For the stable operation of optoelectronic devices, strong adhesion of graphene conductive films to substrates is essentially needed. In particular, touch screen panels, which are operated by mechanical friction, require strong surface strength to enable long-term stability. Passivation with a top coating can be the solution to this problem in that it can protect the surface of graphene films and improve their adhesion to the substrates. In addition, this coating layer can improve the durability of the doped graphene films because it can protect them from the adsorption of moisture and other chemical molecules after chemical treatment to increase the conductivity of the graphene films. However, the process of uniformly coating the insulating layer on the conductive graphene films without considerably decaying the conductivity is challenging. In this paper, we characterize the wettability and surface strength of the top coated insulating layers on graphene films. In addition, we presented that thin insulating polymer layers effectively protect graphene films from external friction forces through the mechanical friction test.

* Address correspondence to ahnj@skku.edu.

Received for review October 11, 2011 and accepted December 12, 2011.

Published online December 12, 2011
10.1021/nn203923n

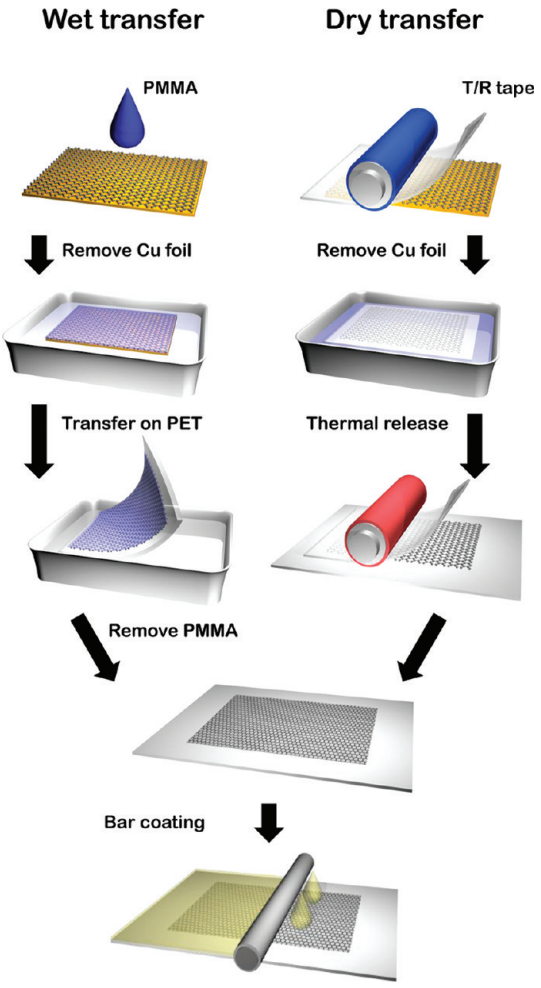

Figure 1. The schematic illustration of graphene transfer (wet and dry transfer) process and subsequent bar-coating process.

RESULTS AND DISCUSSION

Uniformity and Optical Property of the Monolayer Graphene after Bar-Coating Application. The entire fabrication process is shown in the schematic illustration (Figure 1). Once the monolayer graphene was grown on Cu foil, two methods, wet transfer and dry transfer, were applied to transfer the graphene to the target substrates. In the wet transfer procedure, the graphene film was released *via* protection of the graphene film with PMMA and etching the underlying Cu catalyst with ammonium persulphate solution. The film was subsequently transferred onto the desired substrate, *e.g.*, Si wafer or PET substrate, and the support PMMA layer was dissolved and removed by acetone. In the case of dry transfer, a thermal release tape (Jinsung Chemical Co. or Nitto Denko Co.) was attached on the top of graphene by a roll process with soft pressure of around 0.2 MPa. Then, Cu catalyst was etched and rinsed with deionized water and the graphene film was roll-transferred on a desired substrate by exposure to the release temperature of the thermal

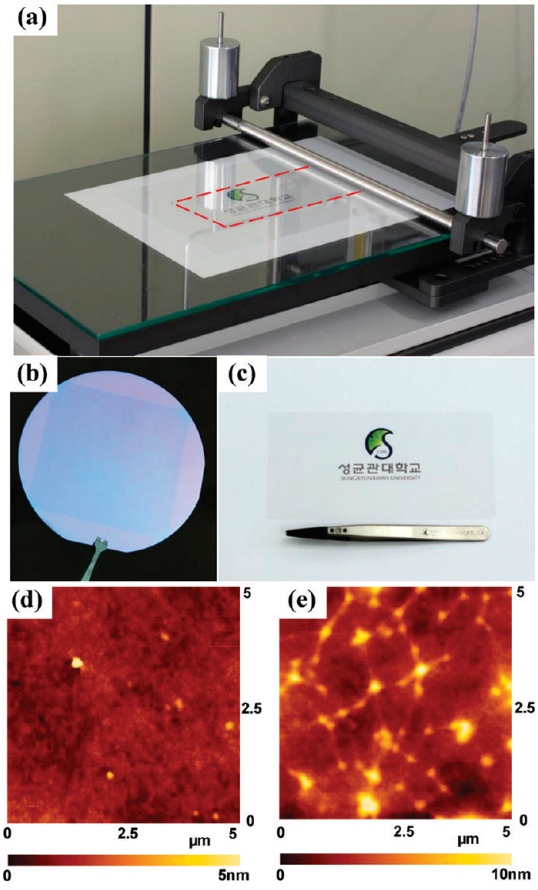

Figure 2. Photographs of bar-coating instrument setup (a) and the resulted polymer thin film on graphene surface on silicon wafer (b) and flexible PET substrate (c). (d,e) AFM morphology of a polymer thin film bar-coated on graphene surface on SiO_2 and PET substrate, respectively.

release tape at *ca.* 90−120 °C with a transfer rate of *ca.* 150−200 mm/min. After the transfer process, a polymer was bar-coated onto the graphene surface with desired thickness.

Figure 2 panels a, b, and c are photographs of the machine setup for bar-coating and the graphene films after bar-coating with P4VP on a 3-in. Si wafer and PET substrate, respectively. As illustrated, large-area monolayer graphene films, wafer scale on SiO_2/Si and 15 × 8 cm^2 on PET, were transferred onto the substrates. Uniform application of the polymer coating layer on the graphene surface was achieved by careful control of the solvent and bar-coating conditions on the Si wafers and PET substrates. Optical microscope was used to observe the uniformity of the bar-coating film on the graphene surface (Figure S1). A 300 nm SiO_2/Si wafer was chosen as the substrate because the monolayer graphene film on it is distinguishable by the color contrast through the optical microscope. To further confirm the uniformity of the bar-coating films on the graphene surfaces, the topography of sample was measured by atomic force microscope (AFM). Figure 2d provides the morphology of a polymer thin layer of P4VP bar-coated on the graphene surface on

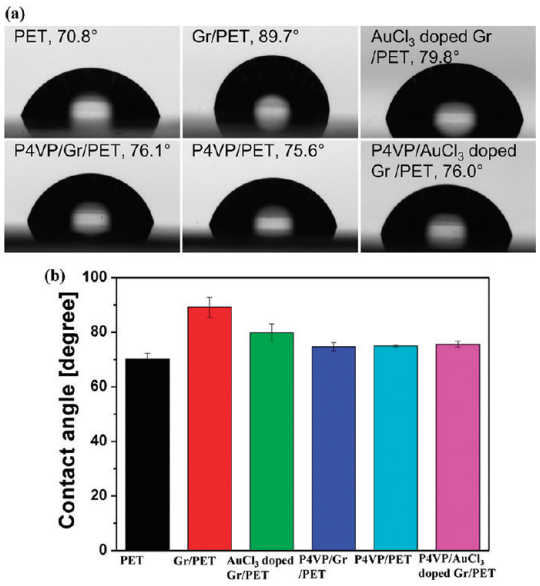

Figure 3. (a) Water contact angles on various sample surfaces: PET, Gr/PET, $AuCl_3$ doped Gr/PET, P4VP/Gr/PET, P4VP/PET, and P4VP/$AuCl_3$ doped Gr/PET. The contact angle values were summarized in panel b.

the SiO_2. After bar-coating with a polymer thin film on the top, both optical imaging and AFM topography indicated that the polymer coating layer was continuous and quite uniform with a smooth surface. The morphology of the polymer coating layer on graphene on the flexible PET substrate was also mapped by AFM and showed slight roughness as well (Figure 2e). A few small dots can come from the shape asperity of the PET substrate. The PET surface has shape asperities with an approximate 10 nanometer height. The bar-coating method obviously provides a direct and effective way to produce large-scale uniform top-coating layers on graphene surfaces.

High transmittance is one of the intrinsic advantages of CVD graphene films, making them excellent candidates for optoelectronic applications, such as transparent electrodes, *etc*. The reported absorbance of monolayer graphene is approximately 2.3%.[20] The pristine monolayer graphene films used in the experiment have a transmittance of ~97.5% at 550 nm on the PET substrate. The transmittance of graphene on the PET substrate before and after polymer thin film of P4VP bar-coating was monitored (Supporting Information, Figure S2). The PET was used as a background, and all samples show extremely small transmittance variation in the 400−850 nm wavenumber regime within error range. Obviously, the polymer coating layer does not affect the optical property of graphene films.

The surface property and uniformity of graphene films after P4VP coating were investigated by the contact angle measurements as well (Figure 3). The contact angle on bare PET substrate was about 70 degrees. After the Cu-grown graphene was transferred

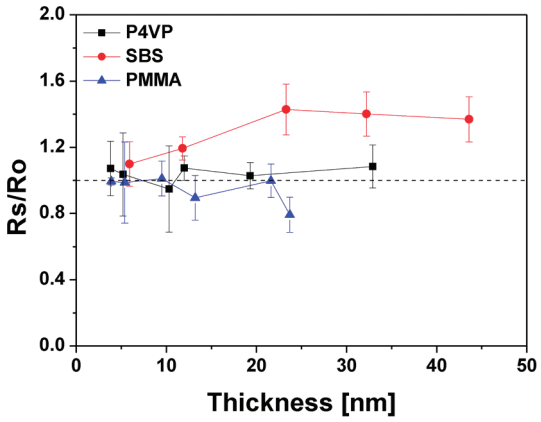

Figure 4. The variation of sheet resistance of graphene films after polymer bar-coated on the top with the thickness of the coated films. R_o and R_s are the sheet resistance of graphene before and after the polymer layer coating.

onto the PET substrate, the contact angle increased to about 90 degrees due to the hydrophobic property of graphene, a finding that is consistent with our recent report.[25] The contact angles on P4VP/Gr/PET and P4VP/PET were almost the same as approximately 76 degrees, indicating that the thin P4VP film was entirely covered on the graphene on PET and dominated the surface property. $AuCl_3$ doping can change the surface property of graphene films. After doping, the contact angle was decrease due to the hydrophilic property of Au^{3+} and Cl^-. When the doped sample was coated with P4VP, the surface property was dominated by P4VP, and the contact angle was found to be similar to other P4VP-covered samples. The results are in accordance with the observations of optical microscopy and AFM.

Evolution of Sheet Resistance by Application of the Polymer Top Coating. Polymer coating layers with different thickness were bar-coated on the top of monolayer graphene thin films by tuning the coating conditions. Various kinds of polymers were applied in the bar-coating process and three kinds of polymers, P4VP, PMMA and SBS, were ultimately selected because of their ability to readily form a uniform thin layer on the graphene surface. The sheet resistance evolution of the graphene films changes with the thickness of top coating layers was elucidated in Figure 4. The sheet resistance of the graphene films bar-coated with SBS gradually increased ~40% in the first 20 nm and reached saturation as the top coating layer thickness increased. The sheet resistance of the films coated with PMMA unexpectedly decreased about 20% with increasing thickness to less than 30 nm. In the case of P4VP, the sheet resistance only has less than 10% fluctuation despite varying the thickness of P4VP. As the thickness of the coating layers was further increased, the graphene films were completely encapsulated and insulated.

Intuitively, the top coating composing insulating polymers would be expected to increase the sheet

resistance of the graphene film due to increased probe contact resistance. The varying tendency of the sheet resistance after coating with the thin polymer layers is thought to be attributed to differing interactions between the coating polymer and the graphene film. It has been suggested that a medium that has good contact with graphene should have a surface tension value of 40−50 mJ/m^2.[26] The hydrophobic interaction and good surface tension match between graphene and SBS (approximately 45 mJ/m^2) are reasonably considered to account for the gradually increasing sheet resistance of the graphene film. PMMA is capable of spreading cross a graphene surface and is widely used as a supporting layer during the graphene transfer process. The PMMA coating layer can minimize cracks of graphene film induced in the transfer process,[27] which is speculated to be responsible for the slightly decreased sheet resistance after coating. P4VP interacts mildly with graphene, and the coating film slightly affects the sheet resistance of the graphene films.

Graphene film has been suggested to be a candidate material for high performance transparent conducting films (TCFs). However, its sheet resistance is still higher than its counterparts of carbon nanotube-based TCF and ITO. It has been reported that $AuCl_3$ chemical doping is an effective way to improve the conductivity of CVD-grown graphene films.[28,29] In the present work, $AuCl_3$ in nitromethane at a concentration of 0.025 M was used to dope the graphene films, while the sheet resistance was reduced by ~86% from an average of 792 Ω/sq of the pristine samples to 111 Ω/sq after 10-min $AuCl_3$ doping (Supporting Information, Figure S3). The sheet resistance of graphene films was dramatically dropped by $AuCl_3$ doping and was almost saturated after 0.5 min doping and kept stable even after 15 min doping (Figure S3). The transmittance after doping was decreased by ~2%. The significant drop in sheet resistance was interpreted as an extraction of electrons from the graphene due to the reduction of Au^{3+} to Au^0 (XPS was presented in Supporting Information, Figure S4); therefore, the hole carrier concentration increased. The low sheet resistance and intrinsically high transmittance of doped monolayer graphene make it very competitive compared with ITO electrodes, which have a typical sheet resistance of 5−60 Ω/sq with approximately 85% transmittance.[30]

The doping stability was studied over time. Figure 5a shows the sheet resistance of the $AuCl_3$-doped sample changing with time. In the first few days, the sheet resistance dramatically increased by around 40% for the graphene film after 10-min of $AuCl_3$ doping. Considering that the solvent nitromethane itself is also a dopant for graphene[31] and the hygroscopic property of $AuCl_3$,[32] the rapid increase of sheet resistance may be ascribed to the desorption of nitromethane from graphene and the hygroscopic effect of $AuCl_3$. The sheet resistance gradually rose with time. After 42 days, the sheet resistances increased by approximately 100% and 75% for graphene films that were doped 10 and 0.5 min, respectively. After that, the sheet resistance almost reached saturation and did not increase over time. Graphene films with different doping times

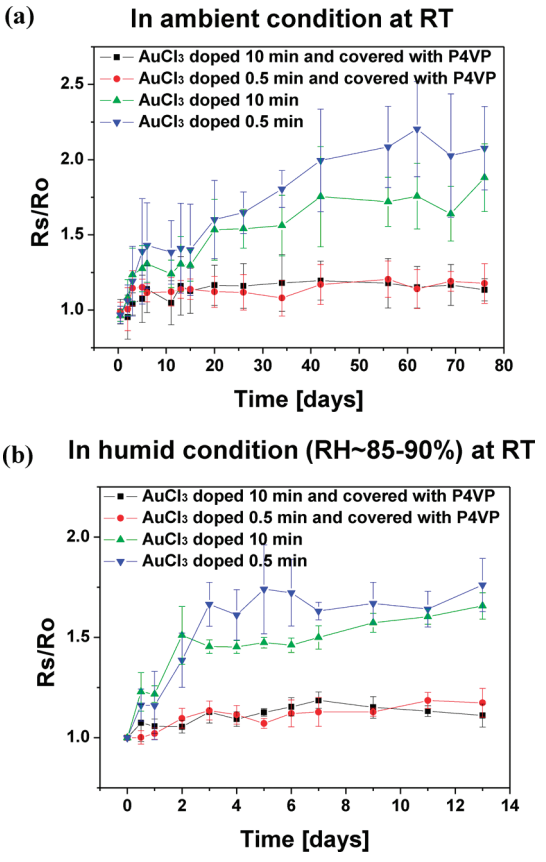

Figure 5. The sheet resistance of $AuCl_3$ doped graphene and $AuCl_3$ doped and covered by cross-linked P4VP changes over time (a) in ambient condition and (b) in a humid circumstance with RH ≈ 85−90% at room temperature (RT).

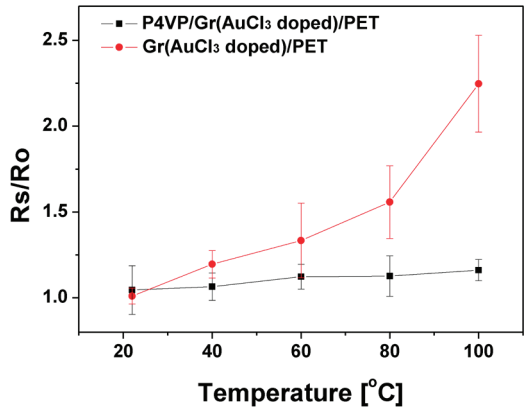

Figure 6. The sheet resistance of $AuCl_3$ doped graphene and $AuCl_3$ doped and covered by cross-linked P4VP changes over temperature. The samples were kept at desired temperature for 6 h and then measured.

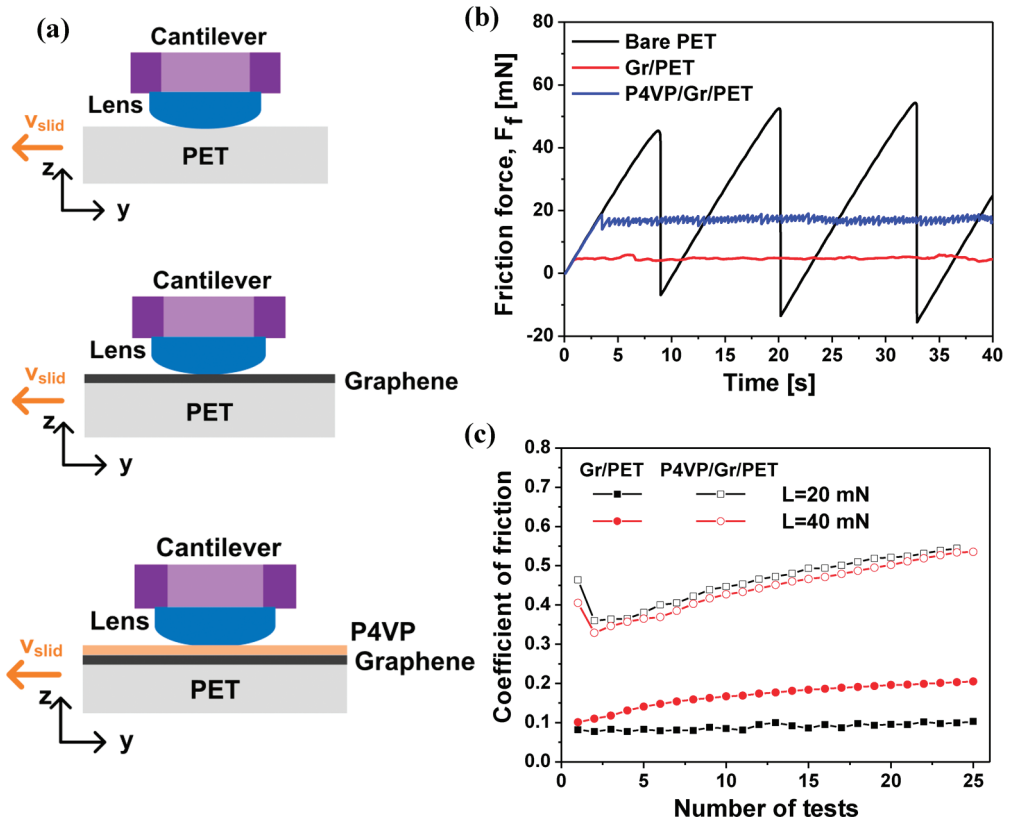

Figure 7. (a) Schematic illustration of friction test. (b) The friction force at different sample surface, PET, Gr/PET, and P4VP/Gr/PET, under the contact load of 40 mN. (c) The coefficient of friction (COF) as a function of the number of friction test on Gr/PET and P4VP/Gr/PET under the contact load of 20 and 40 mN.

showed the same tendency over time as that shown in Figure 5a. After a polymer thin film of P4VP was coated on the top of doped samples, the sheet resistance had an increase of *ca.* 30−40%. However, the doped graphene films with coated polymer thin films exhibited excellent stability in ambient conditions; the sheet resistance had less than 20% variation even after 76 days regardless of doping duration (Figure 5a). The stability may be attributed to the fact that the polymer film inhibits the desorption of nitromethane and hygroscopic process of Cl^- ions.

The capability of protection of the polymer coating layer was further proved by putting samples in a humid circumstance. The doped graphene with a coating layer presented stable sheet resistance values even in a harsh circumstance with a relative humidity (RH) 85−90% at room temperature for 2 weeks (Figure 5b). The sheet resistance variation had a similar tendency with the samples in the ambient condition.

Furthermore, the P4VP coating layer showed excellent temperature stability as shown in Figure 6. The samples were kept at the desired temperature for 6 h and then measured. The sheet resistance of the P4VP encapsulated doped samples retained a small variation of ~10%, while the uncoated samples had increased sheet resistance over temperature. The evolution of sheet resistance over time at 100 °C was also tracked (Supporting Information, Figure S5). The P4VP encapsulated doped sample maintained the property, while the doped sample without coating layer had a rapid increase of sheet resistance over time. The results indicate that the polymer coating layer can provide consistent protection for graphene films.

TABLE 1. Experimental Conditions for the Friction Tests Using a Microtribometer

friction test	
lens (radius of curvature, *R* (mm))	fused silica (7.7)
applied load (mN)	20, 40
max contact pressure[a] (MPa)	9.12−11.5
sliding distance (μm)	2000
sliding speed, v_{slid} (μm/s)	50

[a] The maximum contact pressure was calculated using Hertz's contact theory[33] under the given load. The elastic modulus and Poisson's ratio used in the calculation are 73 GPa and 0.17 for the fused silica lens, and 3 GPa and 0.4 for the PET substrate. The graphene transferred on PET substrate was neglected in the calculation because the thickness of graphene was atomically thin.

Polymer Coating Layer Effects on the Frictional Properties. The friction test is schematically illustrated in Figure 7a. This test was conducted on the surfaces of bare PET, Gr/PET, and P4VP/Gr/PET using a custom-built microtribometer. Table 1 summarizes the test conditions used in the experiment.

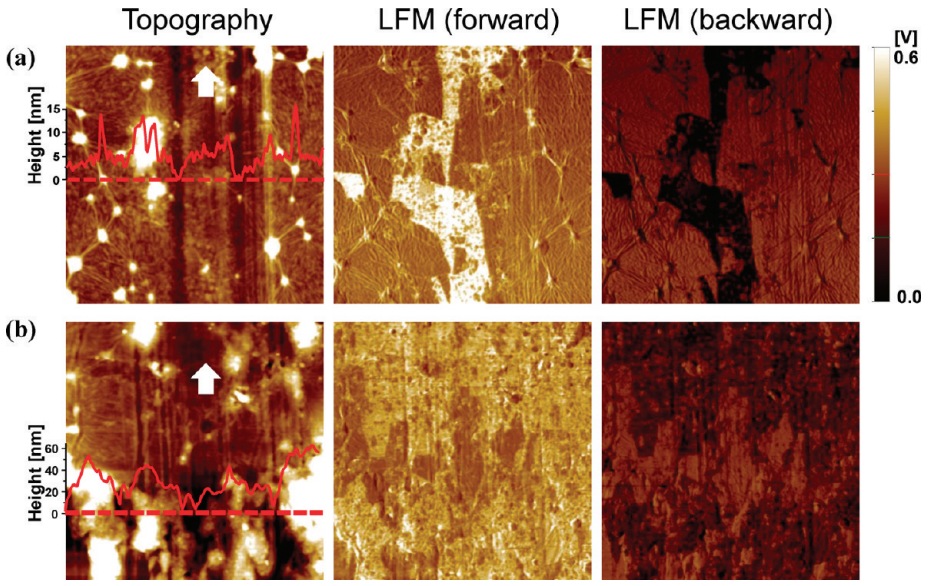

Figure 8. Topography and lateral force microscopy (LFM) images of wear track for Gr/PET (a) and P4VP/Gr/PET (b). The scan size was $4 \times 4\ \mu m^2$ and all LFM images use the same *z*-scale bar. In the topography images, a white arrow indicates the sliding direction.

Figure 7b elucidates the measured friction force over time under the contact load of 40 mN. For bare PET, the friction force was significantly increased and abruptly decreased periodically, called the stick–slip phenomenon. (The stick–slip phenomenon is frequently observed when the glass is slid against a polymer under a low contact pressure.) In contrast, when CVD-grown graphene was coated on the PET surface, the friction force significantly decreased and the stick–slip phenomenon disappeared, indicating that atomically thin graphene transferred onto PET can remarkably affect PET frictional properties. For P4VP/Gr/PET, the friction force increased compared to that for Gr/PET, but a large variation in friction force was not observed. The difference in friction force between Gr/PET and P4VP/Gr/PET implies that the contacting surfaces during sliding were totally different in both cases.

Figure 7c shows the coefficient of friction (COF) as a function of the number of tests. The friction test was repeated 25 times under the given load at the same location. The test location on the sample was changed with the contact load. For Gr/PET, the COF was kept almost constant during the repeated tests under the contact load of 20 mN while the COF was gradually increased under the contact load of 40 mN. It appeared that when the load was 40 mN, the graphene on PET was damaged and partly torn out as shown in Figure 7a as the number of tests increased. For P4VP/Gr/PET, in contrast, the COF was quite high due to the thin P4VP film cover on Gr/PET. In the first run, the friction force is quite high because the P4VP film was first deformed and partly transferred to the lens surface during the sliding. After that point, the COF gradually increased as the number of tests increased. Even under higher contact load, the COF did not change much, indicating that the contacting surfaces during sliding and the wear mechanism were almost the same in both load conditions.

Figure 8 exhibits topography and lateral force microscopy (LFM) images of the wear track for Gr/PET (Figure 8a) and P4VP/Gr/PET (Figure 8b), both of which were obtained by AFM (XE-100, Park Systems, Korea) after the repeated friction test under a load of 40 mN. The scan size was $4 \times 4\ \mu m^2$ and the scan rate was 0.1 Hz. Measurements of all samples were performed using an AFM tip (NSC36C; Park Systems, Korea). All LFM images use the same z-scale bar. In the topography images, a white arrow indicates the sliding direction.

As shown in the topography image of Gr/PET, the graphene transferred onto the PET well covered the substrate due to the flexibility of graphene despite the PET substrate having many sharp surface asperities. After 25 times friction tests, the Gr/PET surface was deformed due to the sliding and the graphene was partly worn from the PET substrate, which can be clearly shown in the LFM images. Because graphene is atomically thin and PET has rough surface, the tear site was not distinguished in the topography image. However, the worn part was clearly shown in the LFM images because of the difference in frictional properties between graphene and PET. The bright regions in the forward scan LFM image (the dark regions in the backward scan LFM image) are the regions with higher friction force, which are the parts where the graphene was worn and PET surface had emerged because the friction force on PET surface is larger than that on Gr/PET. The results show that the graphene was partly worn due to the repeated tests; and that could potentially be one of the reasons for the gradual increase in the friction force with test number under the load of 40 mN.

For P4VP/Gr/PET, the polymer top coating layer plays an important role during the sliding process. As mentioned, the P4VP film was partially deformed and torn and transferred onto the surface of lens in the process of sliding, which is supposed to account for the gradually increase of coefficient of friction with the friction test number. AFM topology shows that the surface became rough due to the sliding and there were some parts where the film was worn and the graphene was emerged as indicated in Figure 8b. The part where the graphene was emerged is clearly shown in the LFM images. The brighter region is the part covered with P4VP and the darker region is the part where the graphene emerged in the forward scan LFM image because the friction force on P4VP film is larger than that on graphene. Clearly, the polymer coating layer remains in the most of the area even after 25 times repeated friction at the harsh condition of contact load of 40 mN. The resistance variations before and after friction were evaluated and little change was found (Supporting Information, Figure S6). The results show that the P4VP film effectively protects the graphene on PET against damage induced by repeated sliding.

CONCLUSIONS

In this paper, we utilized the bar-coating method to produce large-area, uniform polymer thin films on the tops of CVD-grown monolayer graphene films and investigated the optical, electric, and tribological properties of the resultant films. A continuous and uniform coating layer with desired thickness can be achieved by carefully tuning solvent and bar-coating conditions. The controllability is very important for large-scale real application. The thin polymer coating layer did not impair the optical transmittance of the graphene films but did influence sheet resistance depending on the interaction between polymer and graphene. SBS had a stronger interaction with graphene and induced high enhancements in sheet resistance. Soft PMMA chains could pack the defects of graphene films and slightly increase conductivity. Cross-linked P4VP thin film led to a small variation of sheet resistance and protected graphene films. The top coating polymer layer has the proven capability to maintain the conductivity of doped graphene films in ambient conditions even for 2.5 months. In addition, thin polymer layer on graphene on PET (P4VP/Gr/PET) effectively protected graphene films on the substrate and diminished the damage of graphene during the repeated sliding, although the coefficient of friction of P4VP/Gr/PET is higher than that of Gr/PET due to the coating layer at the same test condition. Therefore, the thin polymer film coated on CVD-graphene can contribute to the development of transparent and flexible conductive films with high performance and reliability.

EXPERIMENTAL SECTION

Monolayer graphene synthesis and transfer: The monolayer graphene was synthesized on a Cu catalyst by CVD as the previously reported process.[24] The 25 μm thick Cu foil was inserted into a quartz tube and then heated up to 1000 °C at the ambient pressure with a flow H_2 and Ar. After flowing reaction gas mixtures (CH_4:H_2:Ar = 50:15:1000 sccm) for about 5 min, the sample was rapidly cooled down to room temperature. After the graphene synthesis, the supporting polymer layer of poly(methyl methacrylate) (PMMA) was spin coated on the graphene surface to protect it during the wet chemical etching process. The Cu foil was then etched by ammonium persulphate ($(NH_4)_2S_2O_8$) solution, followed by rinsing with deionized water. At this stage, PMMA-supported graphene is ready to transfer onto the desired substrate, for example, Si wafer or flexible polyethylene teraphthalate (PET) substrate. After the transfer, the PMMA support layer was removed by acetone.

The polymers used as the coating layer in this experiment are PMMA ($M_w \approx 20000$), poly(4-vinylphenol) (P4VP) ($M_w \approx 996000$) and polystyrene-*block*-polyisoprene-*block*-polystryrene (SBS) (styrene 30 wt %). Solvents to dissolve PMMA and SBS were chlorobenze and 2-butanone, respectively. P4VP and poly(melamin-*co*-formaldehyde) methylated (MMF) as a cross-linker was mixed in propylene glycol monomethyl ether acetate (PGMEA). All of the polymer materials and solvents were purchased from Aldrich Sigma and used as received. Various kinds of solutions with different concentrations, from 0.1 to 20 mg/mL, were prepared to fabricate the coating layer at the desired thickness. The P4VP thin films were cross-linked at 150 °C for 30 min. The bar-coating layer thickness can be well controlled by adjustments in solution concentration and bar-coating speed. The thickness of the polymer coating layer was measured by ellipsometer.

A transmission spectrum was obtained using a blank PET substrate as a reference for subtraction by UV–vis–NIR measurement. The sheet resistance of the films was measured using a four-point probe instrument. The sheet resistance was calculated by the following equation:

$$R_s = \frac{\pi}{\ln 2}\frac{V}{I} = 4.5324\frac{V}{I}$$

Doping with $AuCl_3$ was achieved by dropping the $AuCl_3$/nitromethane solution (25 mM) on the surface of graphene for the desired time, followed by drying with a stream of nitrogen. The contact angles were measured with a contact angle meter (DSA-100; Krüss GmbH, Hamburg, Germany) by dropping 2 μL deionized water onto each sample surface.

The instrument setup of the friction test is the same as in the previous report.[25] The friction test was performed on the surfaces of bare PET, graphene on PET (Gr/PET), and P4VP-coated graphene on PET (P4VP/Gr/PET). The counterpart material for the test was fused silica with the radius of curvature of 7.7 mm (PLCX-8.0–7.7-UV; CVI Melles Griot, USA). In the test, the contact load was kept constant as 20 or 40 mN and the lens slid against the samples. The sliding velocity was 50 μm/s and the sliding distance was 2 mm. The maximum contact pressure was approximately 10 MPa.

Acknowledgment. This work was supported by the National Research Foundation of Korea (NRF) (2011-0006268, 2011-0019123, 2011-0017587) and the Center for Nanoscale Mechatronics & Manufacturing, one of the 21st Century Frontier Research Programs (2009K000179) funded by the Ministry of Education, Science and Technology. We thank Dr. Youngbae Park for valuable advice.

Supporting Information Available: Optical image of polymer on graphene on SiO_2 (Figure S1); transmittance of monolayer

graphene bar-coated with different thickness of polymer thin layers on PET substrate (Figure S2); $AuCl_3$ doping effect on the sheet resistance (Figure S3); XPS spectrum of $AuCl_3$ doped graphene (Figure S4); the sheet resistance of $AuCl_3$ doped graphene and $AuCl_3$ doped and covered by cross-linked P4VP changes over temperature (Figure S5); measurement of electrical resistance before and after friction test (Figure S6). This material is available free of charge *via* the Internet at http://pubs.acs.org.

REFERENCES AND NOTES

1. Hu, L.; Kim, H. S.; Lee, J.-Y.; Peumans, P.; Cui, Y. Scalable Coating and Properties of Transparent, Flexible, Silver Nanowire Electrodes. *ACS Nano* **2010**, *4*, 2955–2963.
2. Lee, J.-Y.; Connor, S. T.; Cui, Y.; Peumans, P. Solution-Processed Metal Nanowire Mesh Transparent Electrodes. *Nano Lett.* **2008**, *8*, 689–692.
3. De, S.; Higgins, T. M.; Lyons, P. E.; Doherty, E. M.; Nirmalraj, P. N.; Blau, W. J.; Boland, J. J.; Coleman, J. N. Silver Nanowire Networks as Flexible, Transparent, Conducting Films: Extremely High DC to Optical Conductivity Ratios. *ACS Nano* **2009**, *3*, 1767–1774.
4. Han, J. T.; Kim, J. S.; Jeong, H. D.; Jeong, H. J.; Jeong, S. Y.; Lee, G.-W. Modulating Conductivity, Environmental Stability of Transparent Conducting Nanotube Films on Flexible Substrates by Interfacial Engineering. *ACS Nano* **2010**, *4*, 4551–4558.
5. Wu, Z.; Chen, Z.; Du, X.; Logan, J. M.; Sippel, J.; Nikolou, M.; Kamaras, K.; Reynolds, J. R.; Tanner, D. B.; Hebard, A. F.; Rinzler, A. G. Transparent, Conductive Carbon Nanotube Films. *Science* **2004**, *305*, 1273–1276.
6. Zhang, M.; Fang, S.; Zakhidov, A. A.; Lee, S. B.; Aliev, A. E.; Williams, C. D.; Atkinson, K. R.; Baughman, R. H. Strong, Transparent, Multifunctional, Carbon Nanotube Sheets. *Science* **2005**, *309*, 1215.
7. Doherty, E. M.; De, S.; Lyons, P. E.; Shmeliov, A.; Nirmalraj, P. N.; Scardaci, V.; Joimel, J.; Blau, W. J.; Boland, J. J.; Coleman, J. N. The Spatial Uniformity and Electromechanical Stability of Transparent, Conductive Films of Single Walled Nanotubes. *Carbon* **2009**, *47*, 2466–2473.
8. Leem, D.-S.; Wöbkenberg, P. H.; Huang, J.; Anthopoulos, T. D.; Bradley, D. D. C.; deMello, J. C. Micron-Scale Patterning of High Conductivity Poly(3,4-ethylendioxythiophene): poly(styrenesulfonate) for Organic Field-Effect Transistors. *Org. Electron.* **2010**, *11*, 1307–1312.
9. Huang, J.; Wang, X.; deMello, A. J.; deMello, J. C.; Bradley, D. D. C. Efficient Flexible Polymer Light Emitting Diodes with Conducting Polymer Anodes. *J. Mater. Chem.* **2007**, *17*, 3551–3554.
10. Eda, G.; Fanchini, G.; Chhowalla, M. Large-Area Ultrathin Films of Reduced Graphene Oxide As a Transparent and Flexible Electronic Material. *Nat. Nanotechnol.* **2008**, *3*, 270–274.
11. De, S.; King, P. J.; Lotya, M.; O'Neill, A.; Doherty, E. M.; Hernandez, Y.; Duesberg, G. S.; Coleman, J. N. Flexible, Transparent, Conducting Films of Randomly Stacked Graphene from Surfactant-Stabilized, Oxide-Free Graphene Dispersions. *Small* **2010**, *6*, 458–464.
12. Wu, J.; Agrawal, M.; Becerril, H. c. A.; Bao, Z.; Liu, Z.; Chen, Y.; Peumans, P. Organic Light-Emitting Diodes on Solution-Processed Graphene Transparent Electrodes. *ACS Nano* **2010**, *4*, 43–48.
13. Wang, X.; Zhi, L.; Mullen, K. Transparent, Conductive Graphene Electrodes for Dye-Sensitized Solar Cells. *Nano Lett.* **2008**, *8*, 323–327.
14. Wang, Y.; Chen, X.; Zhong, Y.; Zhu, F.; Loh, K. P. Large Area, Continuous, Few-Layered Graphene As Anodes in Organic Photovoltaic Devices. *Appl. Phys. Lett.* **2009**, *95*, 063302.
15. Gomez De Arco, L.; Zhang, Y.; Schlenker, C. W.; Ryu, K.; Thompson, M. E.; Zhou, C. Continuous, Highly Flexible, and Transparent Graphene Films by Chemical Vapor Deposition for Organic Photovoltaics. *ACS Nano* **2010**, *4*, 2865–2873.
16. Kumar, A.; Zhou, C. The Race To Replace Tin-Doped Indium Oxide: Which Material Will Win? *ACS Nano* **2010**, *4*, 11–14.
17. Geim, A. K. Graphene: Status and Prospects. *Science* **2009**, *324*, 1530–1534.
18. Lee, C.; Wei, X.; Kysar, J. W.; Hone, J. Measurement of the Elastic Properties and Intrinsic Strength of Monolayer Graphene. *Science* **2008**, *321*, 385–388.
19. Bunch, J. S.; van der Zande, A. M.; Verbridge, S. S.; Frank, I. W.; Tanenbaum, D. M.; Parpia, J. M.; Craighead, H. G.; McEuen, P. L. Electromechanical Resonators From Graphene Sheets. *Science* **2007**, *315*, 490.
20. Nair, R. R.; Blake, P.; Grigorenko, A. N.; Novoselov, K. S.; Booth, T. J.; Stauber, T.; Peres, N. M. R.; Geim, A. K. Fine Structure Constant Defines Visual Transparency of Graphene. *Science* **2008**, *320*, 1308.
21. Bae, S.; Kim, H.; Lee, Y.; Xu, X.; Park, J.-S.; Zheng, Y.; Balakrishnan, J.; Lei, T.; Ri Kim, H.; Song, Y. I.; *et al*. Roll-to-Roll Production of 30-in. Graphene Films for Transparent Electrodes. *Nat. Nanotechnol.* **2010**, *5*, 574–578.
22. Kim, K. S.; Zhao, Y.; Jang, H.; Lee, S. Y.; Kim, J. M.; Kim, K. S.; Ahn, J.-H.; Kim, P.; Choi, J.-Y.; Hong, B. H. Large-Scale Pattern Growth of Graphene Films for Stretchable Transparent Electrodes. *Nature* **2009**, *457*, 706–710.
23. Li, X.; Cai, W.; An, J.; Kim, S.; Nah, J.; Yang, D.; Piner, R.; Velamakanni, A.; Jung, I.; Tutuc, E.; Banerjee, S. K.; Colombo, L.; Ruoff, R. S. Large-Area Synthesis of High-Quality and Uniform Graphene Films on Copper Foils. *Science* **2009**, *324*, 1312–1314.
24. Lee, Y.; Bae, S.; Jang, H.; Jang, S.; Zhu, S.-E.; Sim, S. H.; Song, Y. I.; Hong, B. H.; Ahn, J.-H. Wafer-Scale Synthesis and Transfer of Graphene Films. *Nano Lett.* **2010**, *10*, 490–493.
25. Kim, K.-S.; Lee, H.-J.; Lee, C.; Lee, S.-K.; Jang, H.; Ahn, J.-H.; Kim, J.-H.; Lee, H.-J. Chemical Vapor Deposition-Grown Graphene: The Thinnest Solid Lubricant. *ACS Nano* **2011**, *5*, 5107–5114.
26. Hernandez, Y.; Nicolosi, V.; Lotya, M.; Blighe, F. M.; Sun, Z.; De, S.; McGovern, I. T.; Holland, B.; Byrne, M.; Gun'Ko, Y. K.; *et al*. High-Yield Production of Graphene by Liquid-Phase Exfoliation of Graphite. *Nat. Nanotechnol.* **2008**, *3*, 563–568.
27. Li, X.; Zhu, Y.; Cai, W.; Borysiak, M.; Han, B.; Chen, D.; Piner, R. D.; Colombo, L.; Ruoff, R. S. Transfer of Large-Area Graphene Films for High-Performance Transparent Conductive Electrodes. *Nano Lett.* **2009**, *9*, 4359–4363.
28. Ki Kang, K.; Reina, A.; Shi, Y.; Hyesung, P.; Li, L.-J.; Lee, Y. H.; Kong, J. Enhancing the Conductivity of Transparent Graphene Films *via* Doping. *Nanotechnology* **2010**, *21*, 285205.
29. Güneş, F.; Shin, H.-J.; Biswas, C.; Han, G. H.; Kim, E. S.; Chae, S. J.; Choi, J.-Y.; Lee, Y. H. Layer-by-Layer Doping of Few-Layer Graphene Film. *ACS Nano* **2010**, *4*, 4595–4600.
30. Kim, H.; Horwitz, J. S.; Kushto, G.; Pique, A.; Kafafi, Z. H.; Gilmore, C. M.; Chrisey, D. B. Effect of Film Thickness on the Properties of Indium Tin Oxide Thin Films. *J. Appl. Phys.* **2000**, *88*, 6021–6025.
31. Shin, H. J.; Kim, S. M.; Yoon, S. M.; Benayad, A.; Kim, K. K.; Kim, S. J.; Park, H. K.; Choi, J. Y.; Lee, Y. H. Tailoring Electronic Structures of Carbon Nanotubes by Solvent with Electron-Donating and-Withdrawing Groups. *J. Am. Chem. Soc.* **2008**, *130*, 2062–2066.
32. Lee, I. H.; Kim, U. J.; Son, H. B.; Yoon, S. M.; Yao, F.; Yu, W. J.; Duong, D. L.; Choi, J. Y.; Kim, J. M.; Lee, E. H. Hygroscopic Effects on $AuCl_3$-Doped Carbon Nanotubes. *J. Phys. Chem. C* **2010**, *114*, 11618–11622.
33. Johnson, K. L. *Contact Mechanics*; Cambridge University: New York, 1987.